International Journal of Heat and Mass Transfer 51 (2008) 6110–6117

Contents lists available at ScienceDirect

International Journal of Heat and Mass Transfer

journal homepage: www.elsevier.com/locate/ijhmt

Mixed convection MHD flow in a vertical channel: Effects of Joule heating and viscous dissipation

A. Barletta *, M. Celli

Università di Bologna, Dipartimento, di Ingegneria Energetica, Nucleare e del Controllo Ambientale (DIENCA), Laboratorio di Montecuccolino, Via dei Colli, 16, Bologna I-40136, Italy

ARTICLE INFO

Article history:
Received 20 August 2007
Available online 6 June 2008

Keywords:
Mixed convection
Laminar flow
Fully developed regime
Magnetohydrodynamics
Analytical solution

ABSTRACT

Combined forced and free flow in a vertical channel with an adiabatic wall and an isothermal wall is investigated. The laminar, parallel and fully developed regime is considered. A uniform horizontal magnetic field is assumed to be applied to the fluid. The local balance equations are written in a dimensionless form and solved by taking into account the effects of Joule heating and viscous dissipation. The solutions are obtained both analytically by a power series method and numerically. The dimensionless governing parameters affecting the velocity and temperature profiles are the Hartmann number and the ratio between the Grashof number and the Reynolds number. Dual solutions are shown to exist for every value of the Hartmann number within a bounded range of the ratio between the Grashof number and the Reynolds number. Outside this range, no parallel flow solutions of the problem exist.

1. Introduction

Some authors [1–5] have pointed out that the laminar solution of steady natural or mixed convection problems may be not unique. In particular, the existence of dual solutions of boundary value problems describing external flows has been shown in Refs. [1–4]. Recently [5], the following result has been obtained: for fully developed laminar flow in a plane vertical channel with isothermal walls at the same temperature, the local balance equations admit two different solutions for any given value of the volume flow rate. Moreover, in the case of upward mean flow, there exist a maximum value of the volume flow rate above which no laminar parallel flow solution is admitted [5]. The presence of dual solutions is due to the nonlinearity of the balance equations produced by viscous dissipation. Situations in which the fully developed laminar flow in a vertical channel is described by nonlinear balance equations occur, for instance, when a magnetohydrodynamic force is present and the thermal generation due to Joule effect is non negligible. In recent years, much attention has been devoted to the study of magnetohydrodynamic effects on natural and mixed convection flows [6–11]. Indeed, convective flows in the presence of magnetic fields occur in many technical applications, such as, for instance, the optimization of industrial casting of metals [12]. In particular, in [6] an analytical solution for the natural convection in a two-dimensional rectangular cavity has been determined, in the presence of a vertical magnetic field. Pan and Li [7] have studied the mixed convection in a vertical plane channel with a horizontal magnetic field, in conditions of microgravity with a gravitational acceleration that oscillates in time with a sinusoidal law (g-jitter effect). The mixed convection flow in a horizontal circular duct in the presence of a uniform vertical magnetic field has been studied numerically in Ref. [8]. An experimental study on the natural convection of a $Na^{22}K^{78}$ alloy in a cavity with a rectangular section, in the presence of a vertical magnetic field, has been presented by Burr and Müller [9]. These authors have shown that the magnetic field produces a systematic decrease of heat fluxes in the fluid. In Ref. [10], the authors study the mixed convection in a vertical channel by considering the effects of viscous dissipation and of Joule heating. They determine the velocity and the temperature distribution both analytically, by means of a perturbation expansion, and numerically, by a finite difference method. Sposito and Ciofalo [11] have obtained analytical solutions of the local balance equations for fully developed mixed convection in a vertical plane channel, by considering isothermal walls and several electric boundary conditions.

In this paper, the steady laminar flow of an electrically conducting fluid in a plane vertical channel is considered. The velocity field is parallel to the gravitational acceleration and is orthogonal to the external magnetic field; the latter is uniform and is not influenced by the fluid flow. One of the channel walls is adiabatic, while the other is isothermal. The local balance equations are nonlinear and the boundary value problem, solved analytically, presents two different solutions for each value of the prescribed pressure gradient, provided that the latter lies within a bounded range outside which no laminar and parallel solution exists.

* Corresponding author.
E-mail address: antonio.barletta@mail.ing.unibo.it (A. Barletta).

0017-9310/$ - see front matter © 2008 Elsevier Ltd. All rights reserved.
doi:10.1016/j.ijheatmasstransfer.2008.04.009

Nomenclature

A_n	series coefficients
$\vec{B}$	magnetic induction field
B	modulus of $\vec{B}$
$\vec{E}$	induced electric field
$\vec{f}$	magnetic body force
$\vec{g}$	acceleration due to the gravity
g	modulus of $\vec{g}$
Gr	Grashof number, Eq. (12)
$\vec{J}$	current density
k	thermal conductivity of the fluid
L	channel width
M	Hartmann number, Eq. (12)
P	hydrodynamic pressure, $p+\rho gX$
q_g	power generated per unit volume
Re	Reynolds number, Eq. (12)
T	temperature
T_w	wall temperature
T_{ref}	reference temperature
u	dimensionless velocity
$\vec{U}$	velocity
U	vertical velocity component
U_r	reference velocity, Eq. (13)
X	vertical Cartesian coordinate
Y	horizontal Cartesian coordinate
y	dimensionless coordinate, Eq. (12)

Greek symbols

α	slope of $u(y)$ at $y=0$, Eq. (16)
β	volumetric coefficient of thermal expansion
ΔT	temperature scale, Eq. (13)
ϕ	dimensionless flux, Eq. (25)
Λ	dimensionless parameter, Eq. (12)
μ	dynamic viscosity
ν	kinematic viscosity
ϑ	dimensionless temperature, Eq. (12)
ρ	mass density
σ	electric conductivity
τ_{XY}	shear stress applied at the wall

Superscripts, subscripts

$'$	derivative with respect to y
$(\pm)$	positive/negative threshold value
cr	threshold value
f	first branch of solutions
JH	Joule heating
l	left branch of solutions
r	right branch of solutions
s	second branch of solutions
VD	viscous dissipation

2. Governing equations

We consider the steady laminar flow of an electrically conducting fluid of electric conductivity σ in a vertical parallel plane channel of width L. The X-axis of the coordinate system is opposite to the gravitational acceleration $\vec{g}$ and the Y-axis is perpendicular to the channel walls which are assumed to be impermeable (see Fig. 1). Flow is parallel so that the velocity is directed along the X-axis. The left wall (at $Y=0$) is insulated (adiabatic) and the right one (at $Y=L$) is kept at the constant temperature T_w. The fluid motion is driven simultaneously by an applied pressure gradient, the buoyancy force and the MHD force due to a uniform external magnetic induction field $\vec{B}$ perpendicular to the channel walls. No external electric field is applied. Moreover, the magnetic Reynolds number is so small that the magnetic field induced by the moving fluid is negligible with respect to the external magnetic field.

The induced electric field is $\vec{E}=\vec{U}\times\vec{B}$, so that the current density is given by

$$\vec{J}=\sigma\vec{E}=\sigma\,\vec{U}\times\vec{B}, \tag{1}$$

where σ is the electric conductivity of the fluid, which will be considered as constant. Since $\vec{B}$ is orthogonal to $\vec{U}$ the magnetic body force per unit volume can be expressed as

$$\vec{f}=-\sigma B^2\vec{U}. \tag{2}$$

The power per unit volume generated by Joule effect is

$$q_g=\vec{J}\cdot\vec{E}=\sigma(\vec{U}\times\vec{B})\cdot(\vec{U}\times\vec{B})=\sigma B^2U^2. \tag{3}$$

Let us denote by ρ the density at the reference temperature T_{ref}. The fully developed parallel flow condition and the uniform wall temperature imply that the fluid velocity U along X and the fluid temperature T depend only on Y, the hydrodynamic pressure $P=p+\rho gX$ depends only on X and $\mathrm{d}P/\mathrm{d}X$ is constant. We also assume that the Boussinesq approximation holds and that both the Joule heating and the heat generation by viscous dissipation must be taken into account. The momentum and energy equations can be expressed as

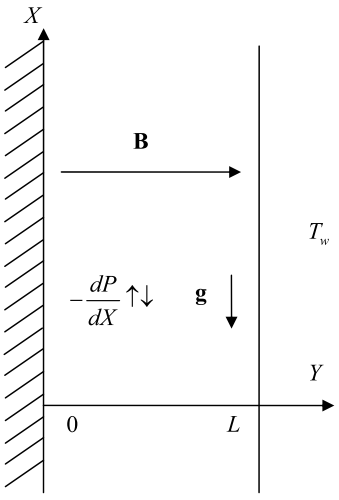

Fig. 1. Drawing of the vertical channel.

$$\mu\frac{\mathrm{d}^2U}{\mathrm{d}Y^2}-\sigma B^2U+\rho g\beta(T-T_{ref})-\frac{\mathrm{d}P}{\mathrm{d}X}=0, \tag{4}$$

$$k\frac{\mathrm{d}^2T}{\mathrm{d}Y^2}+\sigma B^2U^2+\mu\left(\frac{\mathrm{d}U}{\mathrm{d}Y}\right)^2=0. \tag{5}$$

The reference temperature T_{ref} is chosen equal to the temperature $T(0)$ of the adiabatic wall. According to the Boussinesq approximation, the values of ρ, μ, β, k and σ are taken at the reference temperature T_{ref}. The no slip conditions and the prescribed thermal boundary conditions are given by

$$U(0)=U(L)=0, \tag{6}$$

$$\left.\frac{\mathrm{d}T}{\mathrm{d}Y}\right|_{Y=0}=0,\quad T(L)=T_w. \tag{7}$$

From Eq. (4), the temperature $T(Y)$ can be expressed as

$$T(Y) = T(0) + \frac{1}{\rho g \beta}\left(\sigma B^2 U - \mu \frac{\mathrm{d}^2 U}{\mathrm{d}Y^2} + \frac{\mathrm{d}P}{\mathrm{d}X}\right). \tag{8}$$

Differentiating two times Eq. (8) with respect to Y and substituting in Eq. (5), one obtains for the velocity U the non linear ordinary differential equation of the fourth order,

$$\frac{\mathrm{d}^4 U}{\mathrm{d}Y^4} - \frac{\sigma B^2}{\mu}\left(\frac{\mathrm{d}^2 U}{\mathrm{d}Y^2} + \frac{\rho g \beta}{k} U^2\right) - \frac{\rho g \beta}{k}\left(\frac{\mathrm{d}U}{\mathrm{d}Y}\right)^2 = 0. \tag{9}$$

Further boundary conditions on $U(Y)$ can be obtained from Eqs. (6)–(8)

$$\left.\frac{d^2 U}{dY^2}\right|_{Y=0} = \frac{1}{\mu}\frac{\mathrm{d}P}{\mathrm{d}X}, \tag{10}$$

$$\left.\frac{\mathrm{d}^3 U}{\mathrm{d}Y^3}\right|_{Y=0} = \frac{\sigma B^2}{\mu}\left.\frac{\mathrm{d}U}{\mathrm{d}Y}\right|_{Y=0}. \tag{11}$$

3. Dimensionless quantities

Let us define the dimensionless quantities

$$y = \frac{Y}{L}, \quad u(y) = \frac{U(Y)}{U_\mathrm{r}}, \quad \vartheta(y) = \frac{T(Y) - T(0)}{\Delta T},$$
$$Re = \frac{L U_\mathrm{r}}{\nu}, \quad Gr = \frac{g\beta L^3 \Delta T}{\nu^2}, \quad M = \sqrt{\frac{\sigma}{\mu}} BL, \quad \Lambda = \frac{Gr}{Re} = -\frac{g\beta L^4}{\nu k}\frac{\mathrm{d}P}{\mathrm{d}X}, \tag{12}$$

where the velocity and temperature scales are defined as

$$U_\mathrm{r} = -\frac{L^2}{\mu}\frac{\mathrm{d}P}{\mathrm{d}X}, \quad \Delta T = \frac{\mu U_\mathrm{r}^2}{k}. \tag{13}$$

On account of Eq. (12), Eqs. (9)–(11) and the no-slip condition at $Y = 0$ can be rewritten in the dimensionless form

$$u'''' - M^2(u'' + \Lambda u^2) - \Lambda u'^2 = 0, \tag{14}$$

$$u(0) = 0, u''(0) = -1, u'''(0) = M^2 u'(0), \tag{15}$$

where prime denotes differentiation with respect to y. Eqs. (14), and (15) represent an incompletely defined initial value problem, since no initial condition at $y = 0$ for $u'(y)$ is assigned. This problem can be completed by defining a parameter α such that

$$u'(0) = \alpha. \tag{16}$$

The guessed value of α can be obtained once the completed initial value problem has been solved, by prescribing the no-slip boundary condition at $Y = L$, namely

$$u(1) = 0. \tag{17}$$

On account of the Eqs. (12) and (13), the shear stresses applied to the channel walls can be evaluated as

$$\tau_{XY}(0) = \mu\left.\frac{\mathrm{d}U}{\mathrm{d}Y}\right|_{Y=0} = -L\frac{\mathrm{d}P}{\mathrm{d}X}u'(0) = -L\frac{\mathrm{d}P}{\mathrm{d}X}\alpha, \tag{18}$$

$$\tau_{XY}(L) = -\mu\left.\frac{\mathrm{d}U}{\mathrm{d}Y}\right|_{Y=L} = L\frac{\mathrm{d}P}{\mathrm{d}X}u'(1). \tag{19}$$

Eq. (18) clearly shows the physical meaning of parameter α defined in Eq. (16). From Eqs. (8), (12) and (13), the dimensionless temperature $\vartheta(y)$ can be evaluated from the solution of Eqs. (14)–(17), namely

$$\vartheta = \frac{1}{\Lambda}\left(M^2 u - u'' - 1\right). \tag{20}$$

To study the thermal behaviour of the left wall, one can obtain from Eq. (12) the temperature at $y = 0$

$$T(0) = T(L) - \vartheta(1)\Delta T = T_\mathrm{w} - \vartheta(1)\Delta T. \tag{21}$$

Eq. (5) can be written in a dimensionless form as

$$\vartheta'' + M^2 u^2 + u'^2 = 0. \tag{22}$$

Therefore, by integrating Eq. (22) with respect to y in the interval $[0, 1]$ and by employing Eq. (7), one obtains

$$-\vartheta'(1) = M^2\int_0^1 u^2 \mathrm{d}y + \int_0^1 u'^2 \mathrm{d}y. \tag{23}$$

The left hand side of Eq. (23) represents the dimensionless heat flux exchanged through the boundary $y = 1$ while the two integral contributions on the right hand side represent the Joule heating power and the viscous dissipation power generated in the channel, respectively. To explicit the physical significance of the different terms of the Eq. (23), this equation can be rewritten as

$$\phi = \phi_\mathrm{JH} + \phi_\mathrm{VD}, \tag{24}$$

where

$$\phi = -\vartheta'(1), \phi_\mathrm{JH} = M^2\int_0^1 u^2 \,\mathrm{d}y, \phi_\mathrm{VD} = \int_0^1 u'^2 \,\mathrm{d}y. \tag{25}$$

4. Analytical solution

4.1. Special case $\Lambda \to 0$

When Λ becomes negligibly small in correspondence to a non-vanishing value of $\mathrm{d}P/\mathrm{d}X$, the effect of buoyancy in the local balance equations disappears. In this case, forced convection regime occurs. The dimensionless velocity profile is obtained analytically by solving Eqs. (4) and (6) and by employing the dimensionless quantities defined in Eq. (12), namely

$$u(y) = \frac{1}{M^2} - \frac{1}{M^2}\cosh(My) + \frac{\tanh(M/2)}{M^2}\sinh(My). \tag{26}$$

The right hand side of Eq. (26) represents the well known Hartmann–Poiseuille velocity profile. By substituting the Hartmann–Poiseuille profile in Eq. (22), according to the thermal boundary conditions Eq. (7), one obtains the dimensionless temperature profile

$$\vartheta(y) = -\frac{M^2 y^2 + \left(M^2 y^2 + 3\right)\cosh(M) - 4\cosh(My) + 4}{2M^4[\cosh(M) + 1]} + \frac{4\cosh(M - My) + 2My\sinh(M) - \cosh(M - 2My)}{2M^4[\cosh(M) + 1]}. \tag{27}$$

On the other hand, if one solves the initial value problem Eqs. (14)–(16), one obtains, in the limit $\Lambda \to 0$, the dimensionless velocity profile

$$u(y) = \frac{1}{M^2} - \frac{1}{M^2}\cosh(My) + \frac{\alpha}{M}\sinh(My). \tag{28}$$

Eq. (28) implies a linear relation between the velocity in $y = 1$ and α, namely

$$u(1) = \frac{1}{M^2} - \frac{1}{M^2}\cosh M + \frac{\alpha}{M}\sinh M. \tag{29}$$

The no-slip condition at $y = 1$ expressed in Eq. (17) allows one to determine the value of α,

$$\alpha = \frac{\tanh(M/2)}{M}, \tag{30}$$

that makes Eq. (28) congruent with the Hartmann–Poiseuille velocity profile given by Eq. (26).

4.2. Power series solution

In the general case, when buoyancy effects are included, the solution of Eqs. (14)–(16) can be sought in the form of a power series with respect to y,

$$u(y) = \sum_{n=0}^{\infty} A_n y^n. \tag{31}$$

The coefficients A_0, A_1, A_2 and A_3 are easily determined from the initial conditions Eqs. (15) and (16),

$$A_0 = 0, \quad A_1 = \alpha, \quad A_2 = -\frac{1}{2}, \quad A_3 = \frac{M^2\alpha}{6}. \tag{32}$$

The coefficients A_n with $n \geqslant 4$ can be obtained recursively by substituting Eq. (31) in Eq. (14). One obtains

$$A_{n+4} = M^2\frac{(n+2)!}{(n+4)!}A_{n+2} + \frac{n!\Lambda}{(n+4)!}\sum_{j=0}^{n}[M^2 A_j A_{n-j} + (j+1)(n-j+1)A_{j+1}A_{n-j+1}]. \tag{33}$$

The coefficients A_4, A_5 and A_6 evaluated through Eq. (33) are given by

$$A_4 = \frac{\Lambda\alpha^2 - M^2}{24}, \quad A_5 = \frac{(M^4 - 2\Lambda)\alpha}{120}, \quad A_6 = \frac{(2 + 5M^2\alpha^2)\Lambda - M^4}{720}. \tag{34}$$

The no-slip condition at the right wall $y = 1$ becomes

$$u(1) = \sum_{n=0}^{\infty} A_n = 0. \tag{35}$$

While Λ and M can be considered as governing parameters whose value is known a priori, the parameter α is not prescribed. As it can be inferred from Eqs. (32) and (33), for any given pair (Λ, M), Eq. (35) can be considered as an equation in the unknown α. In other words, for any prescribed pair (Λ, M), the values of α compatible with the no-slip condition at $y = 1$ are obtained as solution of Eq. (35).

The quantity $u'(1)$ used in Eq. (19) to evaluate the shear stress $\tau_{XY}(L)$ can be written as

$$u'(1) = \sum_{n=0}^{\infty}(n+1)A_{n+1}. \tag{36}$$

Substituting Eq. (31) in Eq. (20), the dimensionless temperature distribution is

$$\vartheta = \frac{1}{\Lambda}\left\{\sum_{n=0}^{\infty}\left[M^2 A_n - (n+1)(n+2)A_{n+2}\right]y^n - 1\right\}. \tag{37}$$

Moreover, substituting Eqs. (31) and (37) in Eq. (25)

$$\phi = \frac{1}{\Lambda}\sum_{n=0}^{\infty}(n+1)[(n+2)(n+3)A_{n+3} - M^2 A_{n+1}], \tag{38}$$

$$\phi_{\mathrm{JH}} = M^2\sum_{n=0}^{\infty}\frac{1}{n+1}\left(\sum_{j=0}^{n}A_j A_{n-j}\right), \tag{39}$$

$$\phi_{\mathrm{VD}} = \sum_{n=0}^{\infty}\frac{1}{n+1}\left(\sum_{j=0}^{n}(j+1)(n-j+1)A_{j+1}A_{n-j+1}\right). \tag{40}$$

5. Discussion of the results

By employing the Euler–Knopp acceleration method [13] (see Appendix), the convergence of the series solution can be enhanced. In Table 1, one can compare the analytical method (truncating the sums to the first 170 terms) with two different numerical methods (explicit Runge–Kutta and Adams predictor–corrector), with reference to quantities α and ϕ. These quantities present dual values for every fixed pair of Λ and M. This table is obtained for $\Lambda = 10$ and different values M. In the following discussion, one will use the terms "right branch" and "left branch" referring to the solutions obtained for the values of α on the right and left intersections with the abscissa axis $u(1) = 0$ of the diagrams in Fig. 2. The right branch of values of both α and ϕ has at least 5 digits accuracy in each case. For α, the left branch has a high accuracy up to $M = 7$ and then the

Table 1
Comparison between analytical series solution (truncated to the first 170 terms) and numerical solutions (Adams method and explicit Runge–Kutta method): dual values of α and ϕ versus M, for $\Lambda = 10$.

M	α_l	ϕ_l	α_r	ϕ_r	Solution method
1	−3.09411	16.3131	0.43079	0.05914	Analytical
	−3.09411	16.3131	0.43079	0.05914	Numerical (Adams)
	−3.09411	16.3131	0.43079	0.05914	Numerical (Explicit Runge–Kutta)
2	−3.14317	31.4515	0.36353	0.04932	Analytical
	−3.14317	31.4515	0.36353	0.04932	Numerical (Adams)
	−3.14317	31.4515	0.36353	0.04932	Numerical (Explicit Runge–Kutta)
3	−3.00281	77.3591	0.29380	0.03848	Analytical
	−3.00281	77.3591	0.29380	0.03848	Numerical (Adams)
	−3.00281	77.3591	0.29380	0.03848	Numerical (Explicit Runge–Kutta)
4	−2.53954	207.874	0.23755	0.02938	Analytical
	−2.53954	207.874	0.23755	0.02938	Numerical (Adams)
	−2.53954	207.874	0.23755	0.02938	Numerical (Explicit Runge–Kutta)
5	−1.84207	541.041	0.19578	0.02255	Analytical
	−1.84207	541.041	0.19578	0.02255	Numerical (Adams)
	−1.84207	541.041	0.19578	0.02255	Numerical (Explicit Runge–Kutta)
6	−1.15349	1275.06	0.16511	0.01758	Analytical
	−1.15349	1275.96	0.16511	0.01758	Numerical (Adams)
	−1.15349	1275.96	0.16511	0.01758	Numerical (Explicit Runge–Kutta)
7	−0.63464	2732.17	0.14223	0.01398	Analytical
	−0.63465	2700.61	0.14223	0.01398	Numerical (Adams)
	−0.63465	2700.61	0.14223	0.01398	Numerical (Explicit Runge–Kutta)
8	−0.30356	4751.35	0.12472	0.01133	Analytical
	−0.30349	5212.25	0.12472	0.01133	Numerical (Adams)
	−0.30349	5212.25	0.12472	0.01133	Numerical (Explicit Runge–Kutta)

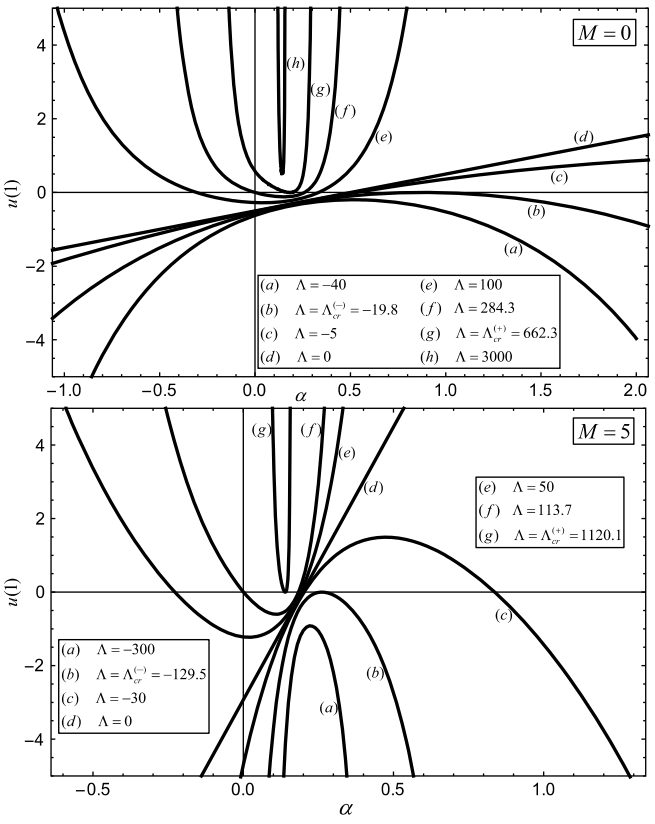

Fig. 2. Plots of $u(1)$ versus α for different values of Λ in the cases $M = 0$ and $M = 5$.

accuracy starts to decrease. For ϕ, the accuracy decreases starting from $M = 6$. The numerical solutions are obtained by solving the initial value problem (14)–(16) with software *Mathematica* (© Wolfram Research, Inc.) through the use of function `NDSolve`. This function allows the user to solve numerically an initial value problem by means of a specified method [14]. The results discussed in the following are based on the power series solution in the case it provides a satisfactory accuracy, otherwise the numerical method is used.

Fig. 2 shows the features of the solution space for different positive and negative values of Λ, with $M = 0$ (absence of MHD effects) and $M = 5$. Both the frames of Fig. 2 are divided in two regions by the $\Lambda = 0$ straight line given by Eq. (29). Note that Eq. (29) in the limiting case $M = 0$ reduces to $u(1) = -1/2 + \alpha$. Fig. 2 reveals that the no-slip condition given by Eq. (17) can be fulfilled only when Λ belongs to the interval $\Lambda_{cr}^{(-)} \leq \Lambda \leq \Lambda_{cr}^{(+)}$. Outside this range of Λ the flow problem does not admit solutions. The dependence of the threshold values $\Lambda_{cr}^{(-)}$ and $\Lambda_{cr}^{(+)}$ on M is represented in Fig. 3. This figure shows that the range of allowed values of Λ expands as M increases. It must be pointed out that, for $\Lambda > 0$, the right branch of solutions corresponds to values of α nearer to that given by Eq. (30). The latter α is the one characteristic of Hartmann–Poiseuille flow. On the other hand, the left branch of solutions represents a marked departure from the Hartmann–Poiseuille flow regime. In the case $\Lambda < 0$, the reverse occurs: the left branch of solutions corresponds to values of α nearer to that given by Eq. (30), while the right branch of solutions markedly departs from the Hartmann–Poiseuille regime. In the following, for $\Lambda > 0$, the right branch of solutions will be denoted as "first branch" while the left branch will be denoted as "second branch". For $\Lambda < 0$, the left branch of solutions will be denoted as "first branch" while the right branch will be denoted as "second branch".

For a given Hartmann number M, there exists an interval $\Lambda_{cr}^{(-)} \leqslant \Lambda \leqslant \Lambda_{cr}^{(+)}$ outside which the boundary value problem (4)–(7) does not admit solutions. When Eqs. (4)–(7) have no solutions, one cannot have parallel flows within the channel. The case $\Lambda < \Lambda_{cr}^{(-)}$ implies a negative Λ with a sufficiently high absolute value, *i.e.*, from Eq. (12), a downward directed pressure force with a sufficiently high value of $|dP/dX|$. The case $\Lambda > \Lambda_{cr}^{(+)}$ implies a sufficiently high positive Λ, i.e., from Eq. (12), an upward directed pressure force with a sufficiently high value of $|dP/dX|$. In other words, whatever is the sign of dP/dX, parallel flow is impossible when $|dP/dX|$ exceeds some threshold value. The impossibility of parallel flow under some parametric conditions implies that other flow regimes will take place instead. It is reasonable to expect that more complicated eddy flow patterns replace the parallel flow when too high pressure gradients are applied to the fluid.

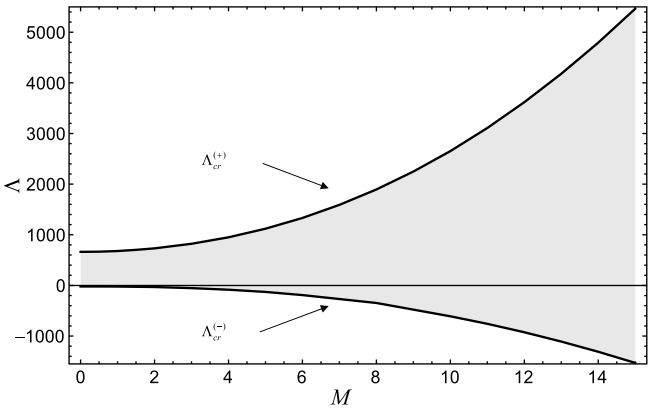

Fig. 3. Threshold values $\Lambda_{cr}^{(\pm)}$ versus M.

Fig. 4 refers to the Hartmann–Poiseuille flow regime ($\Lambda \to 0$), *i.e.* the regime of negligible buoyancy. This figure shows the dimensionless velocity profiles $u(y)$ for different values of M. As is well known, the effect of an increasing Hartmann number is an overall reduction of the fluid velocity.

When the buoyancy effect takes place, the parallel flow solution of the governing equations is in general not unique, as it is revealed by Fig. 2. In the limit $\Lambda \to 0$, $u(y)$ is always positive, thus implying, on account of Eq. (12), that the fluid flow always follows the direction of decreasing pressure. On the other hand, due to the effect of buoyancy, flows in the direction of increasing pressure may take place when $\Lambda \neq 0$; for these flows, $u(y)$ is negative. Obviously, the direction of increasing pressure depends on the sign of Λ, as implied by Eq. (12): a positive value of Λ means that the pressure increases in the downward direction; a negative value of Λ means that the pressure increases in the upward direction. In Fig. 5, dual

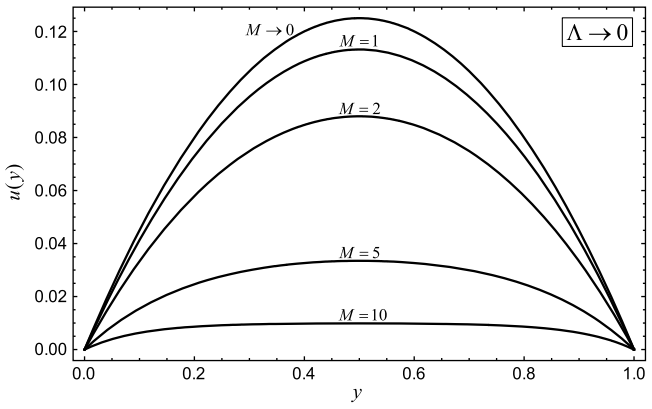

Fig. 4. Plots of Hartmann–Poiseuille flow ($\Lambda \to 0$) profiles $u(y)$ for different values of M.

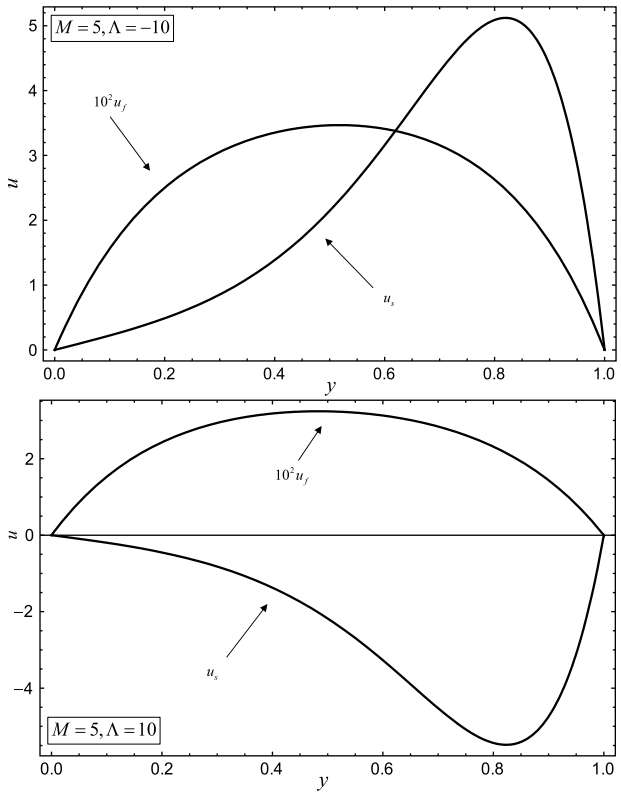

Fig. 5. Dual solutions velocity profiles u versus y for $M = 5$ and $\Lambda = -10$ (upper frame), $M = 5$ and $\Lambda = 10$ (lower frame).

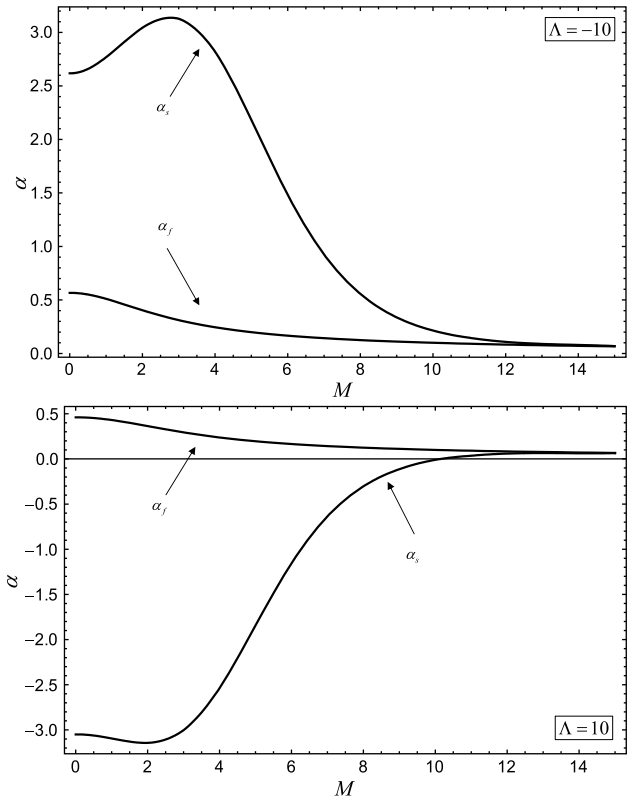

Fig. 6. Plots of the dual velocity gradients at left wall α versus M. $\Lambda = -10$ for the upper frame and $\Lambda = 10$ for the lower frame.

velocity profiles are reported with reference to $M = 5$. These plots of u can be easily interpreted according to the following rule: positive values of u imply that the fluid flows in the direction of decreasing pressure (normal flow), negative values of u imply that the fluid flows in the direction of increasing pressure (reversed flow). Therefore, the lower frame of Fig. 5 shows that for $\Lambda = 10$ the second branch solution corresponds to a condition of reversed flow, while the first branch solution yields a condition of normal flow. The upper frame refers to $\Lambda = -10$ and displays normal flow conditions both for the first branch and the second branch solutions. However, it must be pointed out that the normal flows for $\Lambda = -10$ are directed downward. As expected, both frames of Fig. 5 show that the second branch profile is markedly asymmetric and displays a high velocity gradient at the isothermal wall $y = 1$. The first branch solutions correspond to much lower velocity values and, for this reason, these profiles are magnified by a factor of 10^2 for a better comparison with the others. Figs. 6 and 7 represent the change of the wall strain at $y = 0$ and $y = 1$ as a function of M. Fig. 6 shows that the strain at the left wall may have a non–monotonic behaviour and, in every case, assumes very small values when M is very high. As it is shown in Fig. 7, the strain corresponding to the first branch decreases with M and tends to become very small for $M \to \infty$. The second branch solutions display a strain whose absolute value increases with M. The latter feature is related to the increasing asymmetry of the second branch velocity profiles when M increases. As it is suggested in Fig. 5, this increasing asymmetry implies an increasing absolute value of the velocity gradient at $y = 1$.

The thermal features of the solutions are described by Figs. 8–12. Fig. 8 shows the dual temperature profiles for $M = 5$ in two cases: $\Lambda = -10$ and $\Lambda = 10$. Each profile shows that, as expected, the maximum temperature occurs at the adiabatic wall $y = 0$. The first branch temperature profiles, ϑ_f, display low temperature

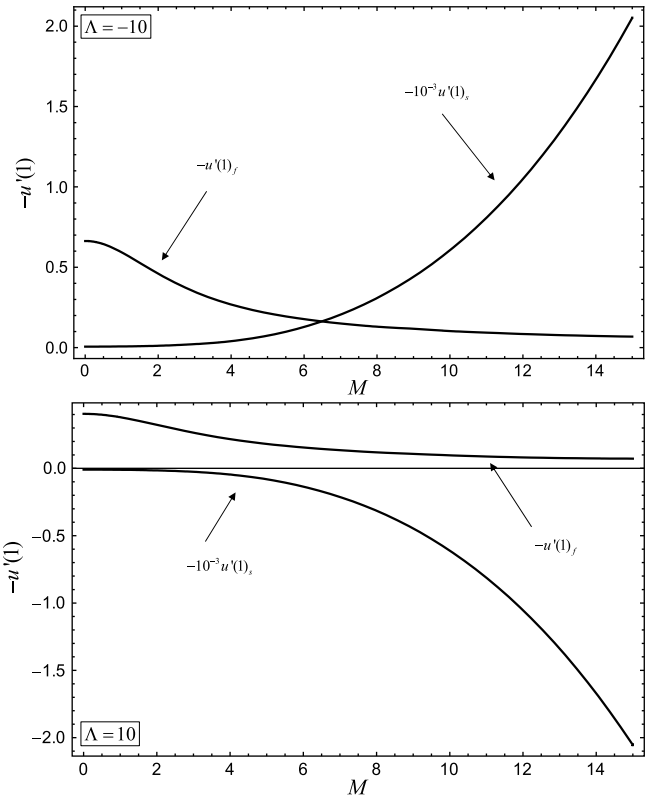

Fig. 7. Plots of the dual velocity gradients at right wall $-u'(1)$ versus M. $\Lambda = -10$ for the upper frame and $\Lambda = 10$ for the lower frame.

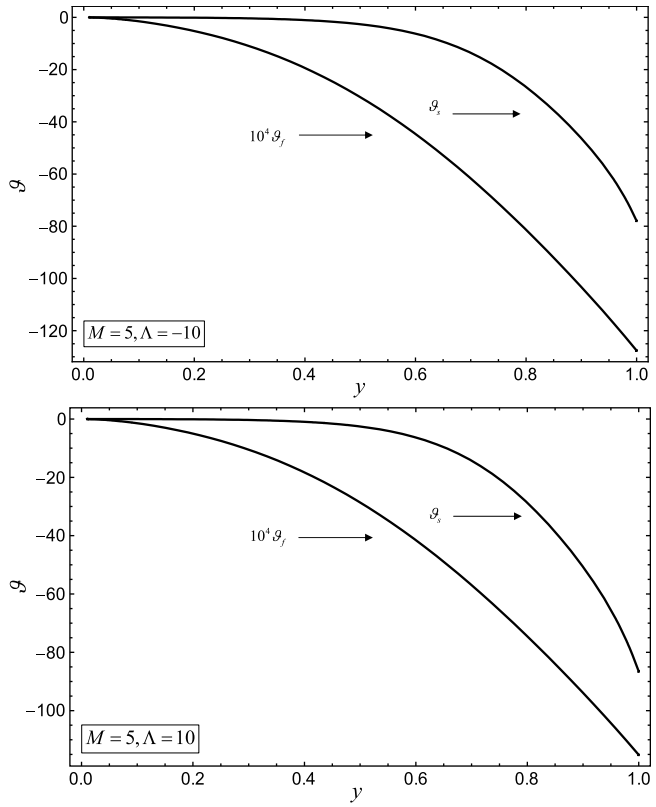

Fig. 8. Dual solutions temperature profiles ϑ versus y for $M = 5$ and $\Lambda = -10$ (upper frame), $M = 5$ and $\Lambda = 10$ (lower frame).

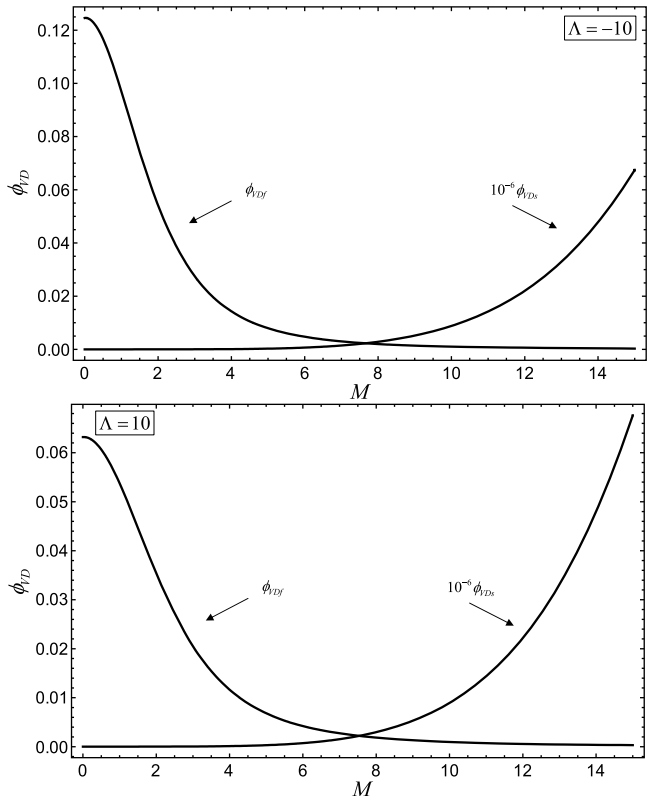

Fig. 10. Plots of dual ϕ_{VD} versus M. $\Lambda = -10$ for the upper frame and $\Lambda = 10$ for the lower frame.

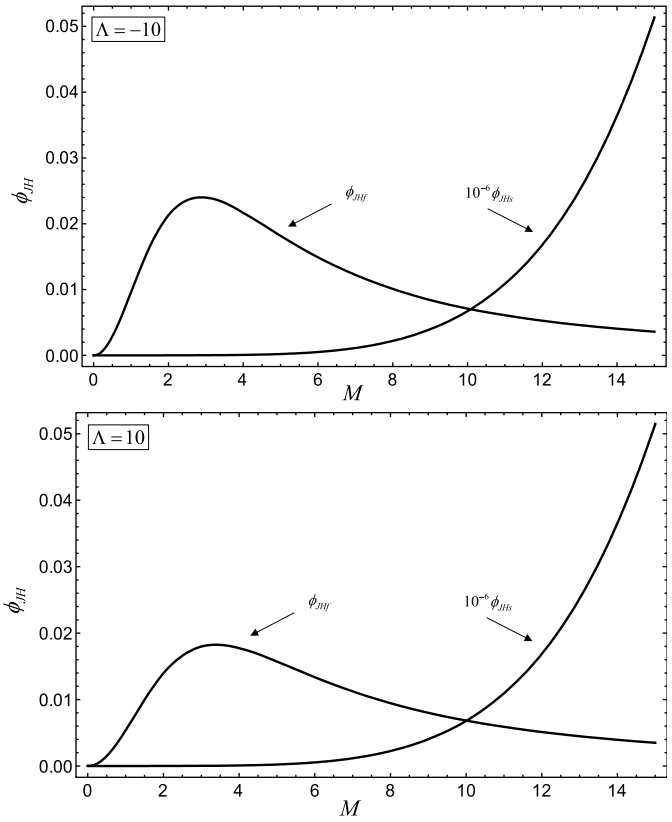

Fig. 9. Plots of dual ϕ_{JH} versus M. $\Lambda = -10$ for the upper frame and $\Lambda = 10$ for the lower frame.

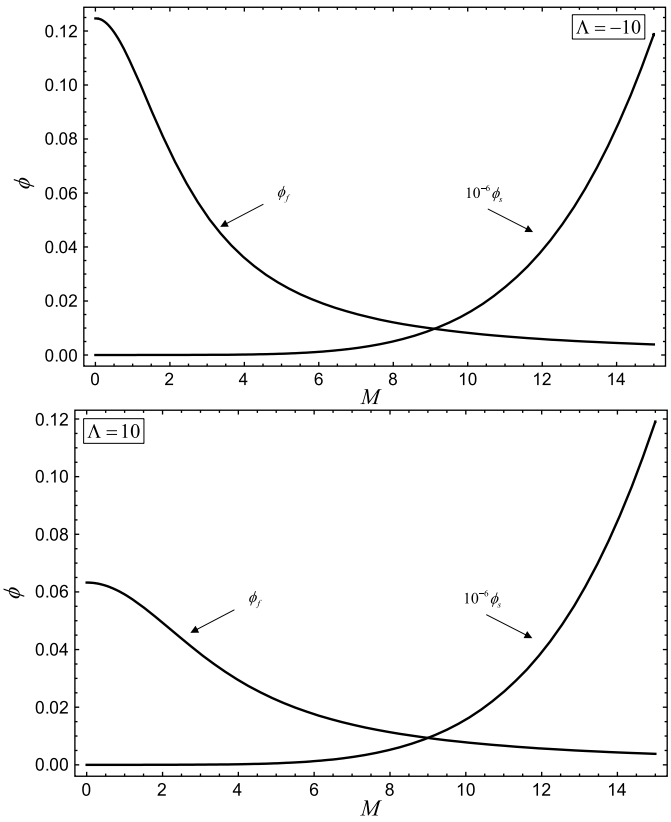

Fig. 11. Plots of dual ϕ versus M at the right wall. $\Lambda = -10$ for the upper frame and $\Lambda = 10$ for the lower frame.

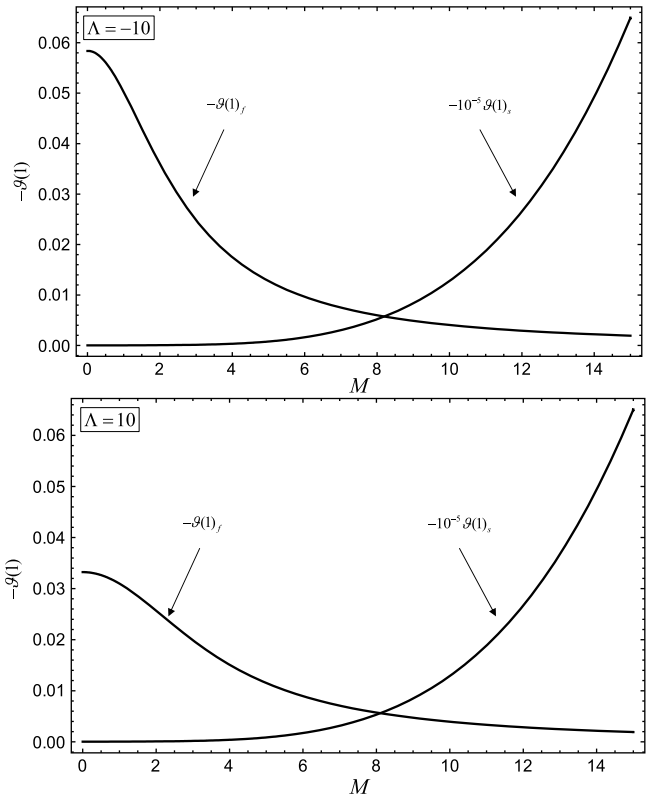

Fig. 12. Plots of dual $-\vartheta(1)$ versus M. $\Lambda = -10$ for the upper frame and $\Lambda = 10$ for the lower frame.

gradients if compared with their dual companions and are thus rescaled by a factor of 10^4. The thermal differences between the dual solutions are compatible with the mechanical differences discussed above, since the second branch solutions always display higher heat generation terms u^2 and u'^2.

Figs. 9–11 describe, respectively, the Joule heat flux contribution, the viscous dissipation heat flux contribution and their sum, ϕ, as a function of M. The latter sum, as it is shown in Eq. (24), represents the wall heat flux at the isothermal boundary $y = 1$. For each figure and frame, the second branch values are rescaled by a factor of 10^{-6} and they are always increasing functions of M. Fig. 9 shows the obvious feature that Joule heating vanishes if $M \to 0$ for each profile. For the first branch of solutions, Φ_{JH} displays a maximum and then it decreases for higher values of M. This feature suggests a stabilizing effect of the magnetic field. Fig. 10 shows that the viscous dissipation flux for the first branch solutions is a monotonic decreasing function of M, thus confirming the stabilizing role of the magnetic field. Figs. 11 and 12 show the behaviour of the wall heat flux at the isothermal wall and of the temperature difference between the boundary walls, respectively. The dependence on M of these quantities is, in fact, qualitatively similar: a monotonic increasing behaviour for the second branch solutions and a monotonic decreasing behaviour for the first branch solutions.

6. Conclusions

Laminar mixed convection in a vertical plane channel has been investigated by taking into account the effect of an external uniform magnetic field orthogonal to the flow direction. Viscous heating and Joule heating in the fluid are considered. The local balance equations have been written in a dimensionless form and solved both analytically by a power series method and numerically. The governing dimensionless parameters are: the Hartmann number M, the ratio Λ between Grashof number Gr and the Reynolds number Re. The main results obtained are the following.

- For every choice of M, the governing equations admit solutions only within a range $\Lambda_{cr}^{(-)} \leqslant \Lambda \leqslant \Lambda_{cr}^{(+)}$. The values $\Lambda_{cr}^{(\pm)}$ depend on M, $\Lambda_{cr}^{(-)}$ is negative and $\Lambda_{cr}^{(+)}$ is positive. The range of existence of the solutions expands with M.
- For fixed values of M and Λ, within the range of existence, two distinct solutions of the governing equations are allowed (dual solutions). The dual solutions become coincident when $\Lambda = \Lambda_{cr}^{(\pm)}$.
- Within each dual solutions pair, one solution is more similar than the other to the Hartmann–Poiseuille flow solution. This feature has been used to distinguish between a first branch solution, more similar to the Hartmann–Poiseuille solution, and a second branch solution, markedly dissimilar from the Hartmann–Poiseuille solution.
- For the second branch of solutions, the absolute value of the strain at the isothermal wall, the heat flux due to viscous dissipation, the heat flux due to Joule heating and the heat flux at the isothermal wall are monotonic increasing functions of M.

Appendix. Euler–Knopp method

Let us consider a converging series,

$$S = \sum_{n=0}^{\infty} w_n. \tag{A.1}$$

Let us define the modified coefficients

$$\tilde{w}_n = \frac{n!}{2^{n+1}} \sum_{j=0}^{n} \frac{w_j}{j!\,(n-j)!}. \tag{A.2}$$

Then, the series

$$\sum_{n=0}^{\infty} \tilde{w}_n \tag{A.3}$$

sums up to S. The modified series (A.3) is thus equivalent to that appearing in Eq. (A.1) although, in several cases, its convergence is much faster.

References

[1] G. Wilks, J.S. Barmley, Dual solutions in mixed convection, In: Proceedings of the Royal Society of Edimburg, Section A (Mathematical and Physical Sciences), vol. 87, part 3–4, 1981, pp. 349–358.
[2] J.H. Merkin, On dual solutions occurring in mixed convection in a porous medium, J. Eng. Math. 20 (1985) 171–179.
[3] T. Mahmood, J.H. Merkin, Similarity solutions in axisymmetric mixed–convection boundary-layer flow, J. Eng. Math. 20 (1) (1988) 73–92.
[4] A. Ridha, Aiding flows non-unique similarity solutions of mixed-convection boundary-layer equations, J. Appl. Math. Phys. (ZAMP) 47 (3) (1996) 341–352.
[5] A. Barletta, E. Magyari, B. Keller, Dual mixed convection flows in a vertical channel, Int. J. Heat Mass Transfer 48 (2005) 4835–4845.
[6] J.P. Garandet, T. Alboussiere, R. Moreau, Buoyancy driven convection in a rectangular enclosure with transverse magnetic field, Int. J. Heat Mass Transfer 35 (1992) 741–748.
[7] B. Pan, B.Q. Li, Effect of magnetic fields on oscillating mixed convection, Int. J. Heat Mass Transfer 41 (1998) 2705–2710.
[8] M.J. Al-Khawaja, R.K. Agarwal, R.A. Gardner, Numerical study of magneto-fluid-mechanic combined free-and-forced convection heat transfer, Int. J. Heat Mass Transfer 42 (1999) 467–475.
[9] U. Burr, U. Müller, Rayleigh–Benard convection in liquid metal layers under the influence of a vertical magnetic field, Phys. Fluids 13 (2001) 3247–3257.
[10] J.C. Umawathi, M.S. Malashetty, Magnetohydrodynamic mixed convection in a vertical channel, Int. J. Non-linear Mech. 40 (2005) 91–101.
[11] G. Sposito, M. Ciofalo, One-dimensional mixed MHD convection, Int. J. Heat Mass Transfer 49 (2006) 2939–2949.
[12] P.A. Davidson, Magnetohydrodynamics in materials processing, Annu. Rev. Fluid Mech. 31 (1999) 273–300.
[13] K. Knopp, Theory and Application of Infinite Series, Dover, New York, 1990.
[14] S. Wolfram, The Mathematica Book, fifth ed., Wolfram Media, 2003.